Directly watching biomolecules in action by high-speed atomic force microscopy

Directly watching biomolecules in action by high-speed atomic force microscopy

Toshio Ando[1,2]
[1]Bio-AFM Frontier Research Center, Institute of Science and Engineering, Kanazawa University, Kakuma-machi, Kanazawa 920-1192, Japan
[2]CREST, Japan Science and Technology Agency, Tokyo 102-0075, Japan

Abstract Proteins are dynamic in nature and work at the single molecule level. Therefore, directly watching protein molecules in dynamic action at high spatiotemporal resolution must be the most straightforward approach to understanding how they function. To make this observation possible, high-speed AFM (HS-AFM) has been developed. Its current performance allows us to film biological molecules at 10−16 frames/s, without disturbing their function. In fact, dynamic structures and processes of various proteins have been successfully visualized, including bacteriorhodopsin responding to light, myosin V walking on actin filaments and even intrinsically disordered proteins undergoing order/disorder transitions. The molecular movies provided insights that could not have been reached in other ways. Moreover, the cantilever tip can be used to manipulate molecules during successive imaging. This capability allows us to observe changes in molecules resulting from dissection or perturbation. This mode of imaging was successfully applied to myosin V, peroxiredoxin and doublet microtubules, leading to new discoveries. Since HS-AFM can be combined with other techniques, such as super-resolution optical microscopy and optical tweezers, the usefulness of HS-AFM will be further expanded in the near future.

Keywords: Imaging · High-speed AFM · Proteins · Dynamic processes · Structural changes

Introduction

Proteins are the structural and functional elements of life. Understanding how proteins produce complex biological architectures and phenomena is one of central issues in life-sciences. To this end, two main approaches have been used: dynamics analysis and structural analysis. Single-molecule biophysical approaches have been devised to detect dynamic behavior of protein molecules (e.g., Deniz et al. 2008; Capitanio and Pavone, 2013). However, the methods are all based on optical techniques, and therefore, can only detect the dynamic behavior of optical markers attached to proteins (i.e. protein molecules themselves are invisible even with super-resolution). X-ray crystallography and NMR have been most instrumental in the structural analysis of proteins at the atomic level. The former is only applicable to crystallized proteins, whereas the latter is applicable to proteins in solution and even in living cells but it is limited to molecular masses smaller than ~40 kDa. Recent advances in cryo-EM have now allowed the determination of atomic structure of proteins from many images of individual molecules in ice (Wang et al 2015). However, the structural information acquired with these three structural methods is limited to static snapshots of proteins. X-ray free electron laser can break this limitation and reveal the time-resolved atomic structure of proteins (Nango et al 2016) but it is only applicable to limited targets.

Under these circumstances, a new microscopy technique is needed that allows direct and dynamic visualization of protein molecules even if the resolution is moderate. Atomic force microscopy (AFM) is a unique, potential candidate for such a technique. AFM allows sub-atomic resolution imaging of flat objects in high vacuum, whereas its resolution is lowered down to a sub-molecular level when AFM is

applied to biological molecules in solution. AFM does not have sufficient time resolution since it takes at least one minute to acquire an image. This is not a theoretical limitation, but a practical one. Efforts to achieve high-speed (HS) AFM were independently initiated around 1993 by the Hansma group (Viani et al 2000) and the Ando group. Practical HS-AFM for biological studies was established around 2008 (Ando et al 2008) following improvements to the first prototype system (Ando et al 2001). Since then, the dynamics of proteins have been successfully visualized (Ando et al 2014). The functionality of HS-AFM is now being expanded in various ways by a combination of other techniques. For example, dynamic phenomena occurring on living cells can also be imaged using a combined HS-AFM/fluorescence microscopy system equipped with a fast wide-area scanner (Watanabe et al 2013; Shibata et al 2015). In this review, I give an overview of the principles, biological applications, and future prospects of HS-AFM.

Imaging rate

For AFM imaging of biological samples, it is common to use the tapping-mode, where the cantilever is excited to oscillate at its first resonant frequency. The oscillating tip intermittently contacts with the surface, resulting in alteration of the cantilever's oscillation amplitude and phase. Deflection of the cantilever is detected with an optical beam deflection (OBD) detector in which a laser beam reflected back from the cantilever illuminates a position-sensitive photodetector (Fig. 1). The laser spot on the photodetector moves up and down as the cantilever oscillates. During the raster-scanning of the sample stage in the XY direction, the amplitude of the cantilever oscillation (and hence, the tip-sample interaction force) is held constant by moving the sample stage in the Z-direction via a feedback control. The feedback signal that is proportional to the scanner Z-displacement is used to form a topography image of the sample surface. Note that the intermittent tip-sample contact avoids the sample being dragged laterally by the tip.

The highest possible imaging rate of AFM is a function of various parameters, as described below (Ando et al 2013). For simplicity, let us assume that the sample has a sinusoidal shape in the XZ plane, characterized with a periodicity λ and a peak height h_0 (Fig. 2). When this sample is scanned in the X-direction with velocity V_s and the feedback controller is switched off, the sample height h under the cantilever tip changes with time as

$$h(t) = \frac{1}{2} h_0 sin(2\pi f t), \qquad (1)$$

where $f \equiv V_s/\lambda$. When the feedback controller is switched on, the Z-scanner is moved sinusoidally at the feedback frequency f in the direction opposite to the sample height. However, because of the chasing-after nature of feedback control, the Z-scanner moves with a time delay τ_0 as

$$Z(t) = -\frac{1}{2} h_0 sin\left(2\pi f t - \theta_0\right), \qquad (2)$$

where $\theta_0 \equiv 2\pi f \tau_0$ is the phase delay of feedback control. Because of this delay, we always have a feedback error ΔZ, which is given by

$$\Delta Z = h(t) + Z(t) = h_0 sin(\theta_0/2) cos(2\pi f t - \theta_0/2) \qquad (3).$$

Due to this error, the tip-sample interaction force varies. The feedback bandwidth f_B is usually defined by the feedback frequency at which $\pi/4$ phase delay occurs, and hence, given by $f_B = 1/(8\tau_0)$. Assuming that the phase delay up to θ_{max} creates no practical problems for the sample, the X-scanner can be scanned at the highest rate $V_s^{max} = \lambda f_B \times (4\theta_{max}/\pi)$. Therefore, the highest possible imaging rate R_{max} is given by

$$R_{max} = 2\theta_{max} \lambda f_B/(\pi W N) \qquad (4),$$

where W is the scan range in the X-direction and N is the number of scan lines. For example, under a realistic condition for imaging protein molecules by our HS-AFM, f_B = 110 kHz, $\theta_{max} = \pi/9$ (i.e., 20°), λ =

10 nm, W = 150 nm and N = 100, *Eq. 4* gives R_{max} = 16.3 frames per second (fps). Note that R_{max} depends on the sample fragility and spatial frequency of the surface corrugation to be detected, $1/\lambda$ in the sample.

As demonstrated in the studies of GroEL–GroES (Yamamoto and Ando 2016) and immunoglobulin G (IgG)–antibody (Preiner et al 2014) interactions, the kinetics or strength of protein-protein interaction can be estimated from successive AFM images. Here, I briefly estimate how strong or weak protein-protein interactions can be measured by HS-AFM imaging. From successive images, we can estimate k_{on} and k_{off} and hence the corresponding dissociation constant K_d in a certain range. For an exponential decay process with a rate constant k, where the probability density function for an unbound or bound state is described as $P(t) = (1/k) \times Exp(-kt)$, AFM imaging has to be performed at least at a frame rate of 4–5 × k/π, considering the Fourier transform of $P(t)$, $1/[1 + (\omega/k)^2]$. Therefore, at the highest possible imaging rate for proteins (~16 fps), the largest k that can be estimated by HS-AFM imaging is 10–12 s^{-1}. On the other hand, it is difficult to observe very slow processes. Stable successive imaging can only be performed for ~10 min. Supposing that ~60 binding or dissociation events are observed during 10 min recording (we need such a number of events in one experiment), the smallest measurable k is ~0.1 s^{-1}. To measure k_{on} (second-order rate constant), we have to change the concentration of one protein in bulk solution, while the counterpart is attached to the substrate surface. When the surface is resistive to non-specific protein binding, we can increase its concentration up to 1 μM or slightly higher as demonstrated (Yamamoto and Ando 2016). Floating molecules in bulk solution do not interfare with AFM imaging, as far as the cantilever tip is not adhesive to the molecules. On the other hand, we can decrease the concentration only down to ~1 nM. Therefore, the measurebale k_{on} by HS-AFM is approxiamtely 10^5–10^{10} $M^{-1}s^{-1}$. Therefore, the K_d that can be estimated by HS-AFM imaging is approximately in the range of 10^{-4}–10^{-11} M under the restrictions of $0.1\ s^{-1} < k_{off} < 12\ s^{-1}$ and $10^5\ M^{-1}s^{-1} < k_{on} < 10^{10}\ M^{-1}s^{-1}$.

Components optimized for HS-AFM

The speed performance of a HS-AFM system (including cantilevers) is defined only by the value of f_B. To increase f_B, the response speed of all devices, particularly mechanical devices (cantilevers and scanners), has to be increased. Moreover, the parasitic oscillations that can be produced by fast displacement of the scanner have to be minimized, and techniques to achieve low-invasive imaging also must be devised. Here, I briefly summarize the major components developed to achieve these conditions. See Ando et al (2008) for a detailed description of instrumentation and Uchihashi et al (2012) for the detailed protocols of HS-AFM imaging.

(1) **Small Si_3N_4 cantilevers**: The cantilever dimensions are 7 μm long, 2 μm wide and 90 nm thick. Their mechanical properties are: resonant frequency f_c = 1.2 MHz in water, quality factor Q_c = 2 in water, and spring constant k_c = 0.2 N/m, resulting in a response time, $Q_c/(\pi f_c)$ = 0.53 μs. As the tip of the small cantilevers is not sharp enough, an electron beam deposited tip is grown on the original tip and then sharpened by plasma etching. Small cantilevers with similar values of k_c and lower values of f_c are commercially available from NanoWorld (f_c = 400 kHz in water) and Olympus (f_c = 600−800 kHz in water).

(2) **Fast amplitude detectors**: The cantilever oscillation amplitude is measured and output by a Fourier method at every cycle of oscillation, using a 100 MHz A/D converter, a field-programmable gate array and a digital signal processor.

(3) **Fast scanners**: High-frequency displacement of a piezo-actuator has a large impact on its supporting mechanism, which tends to generate unwanted mechanical vibrations. To counteract the impulsive force and thereby minimize unwanted vibrations, two identical Z-piezoactuators are placed at a supporting base

in the opposite direction and displaced simultaneously with the same length. To further minimize unwanted vibrations, we developed an active damping technique based on Q-control. The resulting response time of the Z-scanner is 0.5−0.8 μs, comparable to that of the small cantilevers.

(4) **Dynamic proportional-integral-derivative (PID) controllers**: In order to allow weak tip-sample contact, the set point amplitude A_s should be very close to the free oscillation amplitude A_0. However, at this setting, the tip tends to detach from the surface completely at the downhill regions of the surface. Once detached, it takes a long time for the tip to make contact with the surface again, rather like parachuting. To avoid this effect, we developed a dynamic PID controller in which the gain is automatically increased when the downhill regions are scanned (Kodera et al 2006). This method allowed the setting of A_0 = 1−2 nm and $A_s = 0.9 \times A_0$, thus making high-speed imaging compatible with low-invasive imaging.

Impact on sample of tip-sample and surface-sample contacts

In HS-AFM imaging of proteins, the molecules are in contact with the substrate surface and tapped with the oscillating tip many times. Obviously, the molecules are not in their innate condition. Therefore, a question arises whether or not the acquired images really reflect the original structure and behavior of the molecules. The effect of tip-sample contact can be quantitatively assessed as follows. Here, we do not consider the decrease of cantilever oscillation amplitude induced by its resonant frequency shift upon contact with the sample. Therefore, the magnitude of force or the amount of energy described below may be somewhat smaller. Under the conditions usually used for HS-AFM imaging of protein molecules (A_0 = 1−2 nm, $A_s = 0.9 \times A_0$, k_c = 0.1−0.2 N/m and Q_c = 2), the tip-force acting on the sample will on average be: $k_c \times (A_0 - A_s)/Q_c$ = 5−20 pN. Considering a possible feedback error (*Eq. 3*), a larger force (roughly, 40−90 pN) is occasionally exerted on the sample during its uphill stroke. This range of magnitude of force may be too large but the mechanical quantity that affects the sample is not force itself but impulse (force × force-acting time). The force-acting time is very short, ~100 ns or less, because the cantilever is oscillated in Z-direction at ~1 MHz. Therefore, the magnitude of the impulse is less than 10^{-17} N·s per tap. The impact of tip-tapping can also be estimated by the amount of energy transferred from the cantilever to the sample. The cantilever oscillation energy lost at every tip-sample contact, $1/2k_c\,(A_0^2 - A_s^2)/Q_c$, is 0.5–3.8 × 10^{-20} J on average (1.2–9.2 k_BT, where k_B is Boltzmann constant and T is room temperature in Kelvin). The transferred energy, which dissipates quickly, is partitioned among freedoms in the molecule. Even the total amount of energy is identical to or less than the free energy liberated by hydrolysis of one ATP molecule. The lateral force applied from the tip to the sample is negligible. During the tip-sample contact (~100 ns), the sample is dragged by the tip because the sample is scanned in the X direction, relative to the tip. The scan speed is ~2×10^{-4} m/s for a frame rate 10 fps, scan area 100 × 100 nm^2, and the number of scan lines 100. Therefore, the distance by which the sample is dragged in the X-direction is ~0.02 nm or less. Compared to the tip-sample interaction, it is difficult to know *a priori* if the substrate surface would affect the sample. It depends on the sample and phenomenon to be observed. Therefore, we have to judge it from observed results.

HS-AFM imaging of biological molecules in action

AFM can visualize objects only from one direction (perpendicular to the substrate surface). Molecules diffusing very fast on the substrate surface cannot be imaged even with HS-AFM. When two molecules

interacting with each other are immobilized on a substrate, their interaction is restricted. Therefore, to visualize protein molecules in action, we need to optimize assay conditions, including the substrate surface (Yamamoto et al 2010), buffer solution, and the sample itself. By devising assay conditions appropriate for individual specific proteins and phenomena, HS-AFM has had great success in visualizing various proteins in action (see Review Ando et al 2014), as listed in Table 1. Here I briefly highlight some results obtained in my lab and by others (Fig. 3).

Myosin V: The most striking HS-AFM observations were performed using myosin V (M5) (Kodera et al 2010; Kodera and Ando 2014). M5 moves processively on actin filaments with a step size of ~36 nm, in a hand-over-hand manner. These features of M5 motility were deduced mostly from single-molecule optical measurements. However, how the chemical energy of ATP is used during walking has been deduced from ensemble measurements on muscle myosins, and considerd to be basically the same for M5. According to a widely accepted model, the tension for forward movement of M5 is generated when Pi is released from the ADP–Pi-bound leading head upon attachment to actin. This generated tension drives the forward swing of the leading head. Therefore, it has been postulated that the ADP–Pi bound head is in a high-energy state and that upon Pi release this energy is used to drive the lever arm swing as the powerstroke. Therefore, the ADP-bound head is considered to be in a low-energy state. The AFM movies of M5 revealed phenomena inconsistent with this view. In the presence of ATP, the leading head sometimes briefly detached from actin and then reattached, whereas M5 remained at approximately the same position on the filament, like “foot stomping” (Fig. 3a). After foot stomping, the trailing head detached and the leading head swung forwards. The leading head that exhibited foot stomping did not carry bound Pi because Pi had already been released when the head initially attached to actin. This peculiar observation suggests that the ADP-bound head can generate tension and execute a powerstroke. This suggestion was reinforced by another observation. In two-headed bound M5 in the presence of ADP, the coiled-coil tail was occasionally unwound, upon which the leading head swung forwards, very much like a powerstroke observed in the presence of ATP. This observation also suggests that intra-molecular tension can be generated just by binding of the two heads to actin without chemical energy input, and that the lever arm swing of the leading head spontaneously occurs upon trailing head detachment to release this intra-molecular tension. Experiments are now underway to provide direct evidence for this new idea.

Bacteriorhodopsin: The light-driven proton pump bacteriorhodopsin (bR) is the best studied membrane protein. Nevertheless, it dynamic structural change upon light illumination has been elusive. The HS-AFM movie of D96N bR mutant with slow photocycle showed that upon light illumination the cytoplasmic E–F helix portion of each bR displaces outwards by 0.7–0.8 nm (much larger than expected before), resulting in contact with adjacent trimers (Shibata et al 2010). Using different light intensities, the frequency of bR–bR contact was varied. From this observation, it was revealed that this inter-trimer bR–bR contact engenders both positive and negative cooperative effects in the decay kinetics as the initial bR recovers. Further HS-AFM studies of bR successfully revealed how bR molecules form trimers and why the trimer formation is required for the function of bR (Yamashita et al 2013).

F_1-ATPase: The three catalytic β subunits in the rotary motor F_1-ATPase ($\alpha_3\beta_3\gamma$ complex) (Noji et al 1997) change their nucleotide states exclusively, i.e. ATP-free, ADP-bound and ATP-bound states. These three states rotationally propagate in one direction over the β subunits (Boyer 1997). This propagation of the nucleotide states, and hence, the corresponding structural states, drives the rotation of the γ subunit. Because the three β subunits are not in direct contact, a question was raised how they communicate with each other. It was postulated that the γ subunit dictates the nucleotide states through three different β–γ interactions (Wang and Oster, 1998). HS-AFM imaging of the $\alpha_3\beta_3$ subcomplex in the presence of ATP revealed conformational changes in a defined rotary sequence among the three β subunits (Uchihashi et al

2011) (Fig. 3c). Thus, it was concluded that intrinsic cooperativity elicited through the β–β interplay alone is responsible for torque generation to rotate the γ subunit, and therefore, the γ subunit is passively subjected to the torque.

Intrinsically disordered proteins (IDPs): Nearly a half of the entire realm of proteins are disordered either entirely or partly (Uversky et al 2000) but they function as hubs of cellular signaling and regulation in transcription, translation and cell cycle (Wright and Dyson 2015). The structure of IDPs is highly flexible as they dynamically sample a multitude of conformational states. Therefore, structural analysis of IDPs is considerably difficult. In fact, X-ray crystallography and EM have no practical application for IDPs. NMR has been most instrumental in the structural analysis of IDPs but it suffers from the inherent ensemble averaging, and hence can hardly single out the individual structures in the conformational ensemble. HS-AFM can visualize the thin and flexible structure of intrinsically disordered regions (IDRs) in IDPs (Miyagi et al 2008). Some IDRs were observed to transit between fully disordered and partially (or fully) ordered states, whereas other IDRs were always fully disordered (Fig. 3d). Quantitative analyses of HS-AFM images can provide dynamic structural information at the residue level (N. Kodera et al, personal communication).

Chaperonin GroEL: A double ring-shaped GroEL consisting of 14 ATPase subunits assists protein folding, together with co-chaperonin GroES (e.g., Horwich and Fenton 2009). The dynamic GroEL−GroES interaction is actively involved in the chaperonin reaction. Therefore, revealing this dynamic interaction is a key to understanding the operation principle of GroEL. Nevertheless, how this interaction proceeds in the reaction cycle has long been controversial. HS-AFM images of GroEL–GroES interactions in the presence of ATP and substrate protein revealed the occurrence of the primary symmetric GroEL:$GroES_2$ (football complexes) and second-primary asymmetric GroEL:$GroES_1$ (bullet complexes) (Yamamoto and Ando 2016). Thus, the controversial issue is now cleared, demonstrating the importance of direct nano-visualization of dynamic molecular processes. Remarkably, the reaction was observed to often branch into main and side pathways. In the main pathway alternate binding and release of GroES occurs at the two rings, indicating tight cooperation between the two rings. In the side pathway, however, this cooperation is disrupted, resulting in interruption of the alternating rhythm (Fig. 3e). From various properties observed for both pathways, the entire reaction scheme was constructed and a mechanistic insight into the alternate and non-alternate operations of the two-engine system was provided.

Sucrose non-fermenting protein 7 (Snf7): Snf7 is a protein of the endosomal sorting complex required for transport (ESCRT-III). It plays a key role in lipid membrane budding and abscission. HS-AFM of Snf7, when placed on supported planar lipid bilayers, exhibited concentric spiral filament formation (Fig. 3f). When they were disrupted by the cantilever tip, the broken polymers spontaneously formed smaller rings, suggesting a preferred diameter of 25 nm for Snf7 as well as “unbending” of the spiral filaments from their natural curvature (Chiaruttini et al 2015). Thus, it was proposed that in cellular conditions energy would be accumulated during the growth of the spiral spring and eventually released through shrinking of the spiral diameter and buckling of the inner spirals, causing the membrane to buckle, bud and undergo abscission.

As demonstrated in this study, the tip can also be used to manipulate the objects visualized by HS-AFM. Recently, this tip-manipulation technique was refined to precisely specify the loci within the sample to which a controlled strong force is applied. This method has recently been used to detach either head of M5 from actin, break doublet microtubules, and dissect assembled complexes of peroxiredoxin and then observe resulting changes in their behaviour or structure.

Immunoglobulin: Y-shaped IgG has an Fc stem and two identical Fab arms connected to the stem. IgG binds to epitopes on an antigen at the Fab moiety. The antigens are often arranged in lattice patterns on

pathogens, where the epitopes are close to each other. Thus, the question arises: How, and how strongly, do the two Fabs bind to their epitopes? HS-AFM imaging was performed for monoclonal IgG antibodies placed on two-dimensional crystalline protein layers and on a viral capsid (Preiner et al 2014). Monovalent Fab fragments bind to antigens tightly and not to move on the lattice surfaces. On the other hand, divalent antibodies were observed to walk on the lattice surfaces. Therefore, contrary to expectations, divalent binding is weaker than the monovalent binding. This is because a steric strain is imposed to the divalently bound antibodies. This finding will contribute to engineering effective antibodies for therapy and diagnosis.

Other studies: HS-AFM has been applied mostly to purified protein systems but it can also be used to observe higher order structures on the surface of living bacteria and on isolated nuclei. It was first shown in the living bacterium, *Magnetospirillum magneticum* AMB-1, that the surface is covered with a moving net-like structure, mainly composed of porin molecules (Yamashita et al 2012). Similar structures formed by assembled porin were confirmed on the surface of other bacteria (Oestreicher et al 2015).

Recently, the surface of nuclei was observed by HS-AFM (Sakiyama et al 2016). Nuclear pore complexes (NPCs) act as a central regulator of transport between the nucleus and cytoplasm. NPCs consist of ~30 proteins, termed nucleoporins. One third of nucleoporins are intrinsically disordered phenylalanine-glycine strings (FG Nups), which are tethered inside each pore and may play a role in selective barrier and transport mechanism, but this remains elusive. HS-AFM was used to visualize the spatiotemporal dynamics of nucleoporins inside NPCs of *Xenopus laevis* oocytes. The cytoplasmic orifice is circumscribed by highly flexible, dynamically fluctuating FG Nups that rapidly elongate and retract. This transient entanglement in the NPC channel manifests as a central plug when averaged in space and time.

Further progress of high-speed AFM technologies

As highlighted in the above studies, direct visualization of dynamic molecular processes has been a powerful approach. To expand the functionality of HS-AFM, various attempts have been made (see Review Uchihashi et al 2016). The recently achieved wide-area/fast scanner allows the observations of dynamic morphological changes in live cells and protein molecules working on the surfaces of bacteria and nuclei. However, for extremely soft eukaryotic cell surfaces, such high resolution imaging is challenging. This problem is now being solved by the development of high-speed scanning ion conductance microscopy (HS-SICM) that can operate without probe–sample contact. The spatial resolution of SICM is now being improved by developing much sharper capillary probes. Moreover, a tip-scan (not sample stage-scan) HS-AFM system was recently developed, which potentially can be combined with various techniques that use the free space available adjacent to the sample. Tip-scan HS-AFM combined with total internal reflection fluorescence microscopy has already been achieved (Fukuda et al 2013). We are now trying to combine this with optical tweezers to visualize protein molecules under external force. As seen in these examples, HS-AFM, more generally high-speed scanning probe microscopy techniques, will become a major tool in biological research.

Acknowledgments

This work was supported by JST/CREST (#JPMJCR13M1) and KAKENHI from the Ministry of Education, Culture, Sports, Science and Technology, Japan (#21113002, #24227005 and #26119003).

References

Ando T, Kodera N, Takai E, Maruyama D, Saito K, Toda A (2001) A High-speed atomic force microscope for studying biological macromolecules. Proc Natl Acad Sci USA 98:12468–12472

Ando T, Uchihashi T, Fukuma T (2008) High-speed atomic force microscopy for nano-visualization of dynamic biomolecular processes. Prog Surf Sci 83:337–437

Ando T, Uchihashi T, Kodera N (2013) High-speed AFM and applications to biomolecular systems. Annu Rev Biophys 42: 393–414

Ando T, Uchihashi T, Scheuring S (2014) Filming biomolecular processes by high-speed atomic force microscopy. Chem Rev 114:3120–3188

Boyer PD (1997) The ATP synthase--a splendid molecular machine. Annu Rev Biochem 66:717–749

Capitanio M, Pavone FS (2013) Interrogating biology with force: Single molecule high-resolution measurements with optical tweezers. Biophys J 105:1293–1303

Chiaruttini N, Redondo-Morata L, Colom A, Humbert F, Lenz M, Scheuring S, Roux A (2015) Relaxation of loaded ESCRT-III spiral springs drives membrane deformation. Cell 163:1−14

Casuso I, Khao J, Chami M, Paul-Gilloteaux P, Husain M, Duneau J-P, Stahlberg H, Sturgis JN, Scheuring S (2012) Characterization of the motion of membrane proteins using high speed atomic force microscopy. Nat Nanotechnol 7: 525–529

Deniz AA, Mukhopadhyay S, Lemke EA (2008) Single-molecule biophysics: at the interface of biology, physics and chemistry. J R Soc Interface 5:15–45

Eeftens JM, Katan AJ, Kschonsak M, Hassler M, de Wilde L, Dief EM, Haering CH, Dekker C (2016) Condensin Smc2-Smc4 Dimers Are Flexible and Dynamic. Cell Rep 14:1813–1818

Fantner GE, Barbero RJ, Gray DS, Belcher AM (2010) Kinetics of antimicrobial peptide activity measured on individual bacterial cells using high-speed atomic force microscopy. Nat Nanotechnol 5:280–285

Fukuda S, Uchihashi T, Iino R, Okazaki Y, Yoshida M, Igarashi K, Ando T (2013) High-speed atomic force microscope combined with single-molecule fluorescence microscope. Rev Sci Instrum 84:073706 (8 pp)

Hashimoto M, Kodera N, Tsunaka Y, Oda M, Tanimoto M, Ando T, Morikawa K, Tate S (2013) Phosphorylation-coupled intramolecular dynamics of unstructured regions in chromatin remodeler FACT. Biophys J 104:2222–2234

Horwich AL, Fenton WA (2009) Chaperonin-mediated protein folding: using a central cavity to kinetically assist polypeptide chain folding. Q Rev Biophys 42:83−116

Igarashi K, Uchihashi T, Koivula A, Wada M, Kimura S, Okamoto T, Penttilä M, Ando T, Samejima M (2011) Traffic jams reduce hydrolytic efficiency of cellulase on cellulose surface. Science 333:1279–1282

Igarashi K, Uchihashi T, Uchiyama T, Sugimoto H, Wada M, Suzuki K, Sakuda S, Ando T, Watanabe T, Samejima M (2014) Two-way traffic of glycoside hydrolase family 18 processive chitinases on crystalline chitin. Nat Commun 5:3975 (7 pp)

Kodera N, Sakashita M, Ando T (2006) Dynamic proportional-integral-differential controller for high-speed atomic force microscopy. Rev Sci Instrum 77:083704 (7 pp)

Kodera N, Yamamoto D, Ishikawa R, Ando T (2010) Video imaging of walking myosin V by high-speed atomic force microscopy. Nature 468:72–76

Kodera N, Uchida K, Ando T, Aizawa S (2015) Two-ball structure of the flagellar hook-length control protein FliK as revealed by high-speed atomic force microscopy. J Mol Biol 427:406–414

Kodera N, Ando T (2014) The path to visualization of walking myosin V by high-speed atomic force microscopy, Biophys Rev 6:237–260

Kowal J, Chami M, Baumgartner P, Arheit M, Chiu P-L, Rangl M, Scheuring S, Schröder GF, Nimigean CM, Stahlberg H (2014) Ligand-induced structural changes in the cyclic nucleotide-modulated potassium channel MloK1. Nat Communs, 5:3106 (10 pp)

Milhiet P-E, Yamamoto D, Berthoumieu O, Dosset P, Le Grimellec C, Verdier J-M, Marchal S, Ando T (2010) Deciphering the structure, growth and assembly of amyloid-like fibrils using high-speed atomic force microscopy. PLos One 5:e13240 (8 pp)

Miyagi A, Tsunaka Y, Uchihashi T, Mayanagi K, Hirose S, Morikawa K, Ando T (2008) Visualization of intrinsically disordered regions of proteins by high-speed atomic force microscopy. Chem Phys Chem 9:1859−1866

Nango E et al (2016) A three-dimensionalmovie of structural changes in bacteriorhodopsin. Science 354:1552–1557

Ngo KX, Kodera N, Katayama E, Ando T, Uyeda TQP (2015) Cofilin-induced unidirectional cooperative conformational changes in actin filaments revealed by high-speed AFM. e-Life 4:e04806 (22 pp)

Noi K, Yamamoto D, Nishikori S, Arita-Morioka K, Ando T, Ogura T (2013) High-speed atomic force microscopic observation of ATP-dependent rotation of the AAA+ chaperone p97. Structure 21: 1992–2002

Noji H, Yasuda R, Yoshida M, Kinosita Jr K (1997) Direct observation of the rotation of F_1-ATPase. Nature 386:299–302

Oestreicher Z, Taoka A, Fukumori Y (2015) A comparison of the surface nanostructure from two different types of gram-negative cells: Escherichia coli and Rhodobacter sphaeroides. Micron 72:8−14

Preiner J, Kodera N, Tang J, Ebner A, Brameshuber M, Blaas D, Gelbmann N, Gruber HJ, Ando T, Hinterdorfer P (2014) IgGs are made for walking on bacterial and viral surfaces. Nat Commun 5:4394 (8 pp)

Preiner J, Horner A, Karner A, Ollinger N, Siligan C, Pohl P, Hinterdorfer P (2015) High-speed AFM images of thermal motion provide stiffness map of interfacial membrane protein moieties. Nano Lett 15:759–763

Rajendran A, Endo M, Sugiyama H (2015) Direct visualization of walking motions of photocontrolled nanomachine on the DNA nanostructure. Nano Lett 15:6672−6676

Rangl M, Miyagi A, Kowal J, Stahlberg H, Nimigean CM, Scheuring S (2016) Real-time visualization of conformational changes within single MloK1 cyclic nucleotide-modulated channels.Nat Commun 7:12789 (8 pp)

Ruan Y, Miyagi A, Wang X, Chami M, Boudker O, Scheuring S (2017) Direct visualization of glutamate transporter elevator mechanism in substrate transport by high-speed AFM. Proc Natl Acad Sci USA 114:1584–1588

Shibata M, Yamashita H, Uchihashi T, Kandori H, Ando T (2010) High-speed atomic force microscopy shows dynamic molecular processes in photo-activated bacteriorhodopsin. Nat Nanotechnol 5:208 –212

Shibata M, Uchihashi T, Ando T, Yasuda R (2015) Long-tip high-speed atomic force microscopy for nanometer-scale imaging in live cells. Sci Rep 5:8724 (7 pp)

Sakiyama Y, Mazur A, Kapinos LE, Lim RYH (2016) Spatiotemporal dynamics of the nuclear pore complex transport barrier resolved by high-speed atomic force microscopy. Nat Nanotechnol 11:719–723

Shlyakhtenko LS, Lushnikov AY, Miyagi A, Li M, Harris RS, Lyubchenko YL (2013) Atomic force microscopy studies of APOBEC3G oligomerization and dynamics. J Struct Biol 184:217–225

Uchihashi T, Kodera N, Ando T (2012) Guide to video recording of structure dynamics and dynamic processes of proteins by high-speed atomic force microscopy. Nat Protocols 7:1193–1206

Uchihashi T, Watanabe H, Fukuda S, Shibata M, Ando T (2016) Functional extension of high-speed atomic force microscopy. Ultramicroscopy 160:182–196

Uversky VN, Gillespie JR, Fink AL (2000) Why are “natively unfolded” proteins unstructured under physiologic conditions? Proteins 41:415−427

Viani MB, Pietrasanta LI, Thompson JB, Chand A, Gebeshuber IC, Kindt JH, Richter M, Hansma HG and Hansma PK (2000) Probing protein–protein interactions in real time. Nat Struct Biol 7:644–647

Wang RY-R, Kudryashev M, Li X, Egelman EH, Basler M, Cheng Y, Baker D, DiMaio F (2015) *De novo* protein structure determination from near-atomic-resolution cryo-EM maps. Nat Method 12:335–338

Wang H, Oster G (1998) Energy transduction in the F_1 motor of ATP synthase. Nature 396:279–282

Watanabe H, Uchihashi T, Kobashi T, Shibata M, Nishiyama J, Yasuda R, Ando T (2013) Wide-area scanner for high-speed atomic force microscopy, Rev Sci Instrum 84:053702 (10 pp)

Watanabe-Nakayama T, Ono K, Itami M, Takahashi R, Teplow DB, Yamada M (2016) High-speed atomic force microscopy reveals structural dynamics of amyloid β1-42 aggregates. Proc Natl Acad Sci USA 113:5835–5840

Wickham SFJ, Endo M, Katsuda Y, Hidaka K, Bath J, Sugiyama H, Turberfield AJ (2011) Direct observation of stepwise movement of a synthetic molecular transporter. Nat Nanotechnol 6:166–169

Wright PE, Dyson HJ (2015) Intrinsically disordered proteins in cellular signaling and regulation. Nat Rev Mol Cell Biol 16:18−29

Yamamoto D, Uchihashi T, Kodera N, Yamashita H, Nishikori S, Ogura T, Shibata M, Ando T (2010) High-speed atomic force microscopy techniques for observing dynamic biomolecular processes. Methods Enzymol 475 (Part B):541–564

Yamamoto D, Ando T (2016) Chaperonin GroEL-GroES functions as both alternating and non-alternating engines. J Mol Biol 428:3090−3101

Yamamoto H, Fujioka Y, Suzuki SW, Noshiro D, Suzuki H, Kondo-Kakuta C, Kimura Y, Hirano H, Ando T, Noda NN, Ohsumi Y (2016) The Intrinsically disordered protein Atg13 mediates supramolecular assembly of autophagy initiation complexes. Dev Cell 38:86–99

Yamashita H, Taoka A, Uchihashi T, Asano T, Ando T, Fukumori Y (2012) Single molecule imaging on living bacterial cell surface by high-speed AFM. J Mol Biol 422:300−309

Yamashita H, Inoue K, Shibata M, Uchihashi T, Sasaki J, Kandori H, Ando T (2013) Role of trimer-trimer interaction of bacteriorhodopsin studied by optical spectroscopy and high-speed atomic force microscopy. J Struct Biol 184:2–11

Yokokawa M, Takeyasu K (2011) Motion of the Ca^{2+}-pump captured. FEBS J 278:3025–3031

Figure legends

Figure 1. Schematic of tapping-mode atomic force microscope. The cantilever is excited with a piezo to oscillate at the first resonance frequency. Deflections of the cantilever are detected by a position sensor (bi-cell or quadrant photodetector) that is sensitive to the position of the laser spot reflecting back from the cantilever.

Figure 2. Feedback displacement of Z-scanner and error caused by feedback delay. (a) Z-scanner displacement tracing the sample surface with a sinusoidal shape while the sample stage is being scanner in the X-direction with velocity V_s. Black line, sample height change under the tip; red line, Z-scanner trajectory; blue line, tracing error. (b) Change of cantilever oscillation amplitude (blue line). A_0 represents the free oscillation amplitude, while rA_0 ($0 < r < 1$) represents the set point amplitude.

Figure 3. HS-AFM images captured for various protein molecules. (a) Tail-truncated M5 walking on an actin filament, showing forward rotation of the leading lever-arm upon detachment of the trailing head from actin. (b) bR (D96N mutant) responding to green light, showing outwards movement from the trimer centers and resulting contact with bR from adjacent trimers. The light was illuminated at 2 s (green bar) and then switched off. (c) $\alpha_3\beta_3$ subcomplex of F_1-ATPase undergoing conformational changes in the presence of ATP. The height of nucleotide-free β subunit is larger than those containing ATP or ADP. The highest pixel positions marked with red dots shift counterclockwise. At 1.44 s, the α subunit adjacent to the nucleotide-free β subunit appears higher than the β subunit. (d) IDP showing wiggling motion and order/disorder transitions of its IDR. (e) GroEL-GroES interactions showing alternate binding and release of GroES at the two rings of GroEL (3.1−6.4 s). However, this alternating rhythm is interrupted at 7.1 s. (f) Spiral filament formation by polymerization of the ESCRT-III protein Snf7 on a supported lipid membrane. (g) an antibody moving on antigens (Sendai purple membrane). Projection of the Fab arms

onto the membrane surface is indicated by black arrows. The red arrows show positional changes of Fab arms, while the white arrows show no positional change.

Table 1. Various biomolecular and cellular processes visualized by HS-AFM

Motor proteins
Myosin V walking on actin filaments (Kodera et al 2010)
Rotary propagation of chemical and structural states in rotor-less F_1-ATPase (Uchihashi et al 2011)
Membrane proteins
Up-down motion of Glutamate transporter (Ruan et al 2017)
Height change in MloK1 cyclic nucleotide-modulated channels (Kowal et al 2014; Rangl et al 2016)
Spiral spring formation by ESCRT protein (Chiaruttini et al 2015)
Stiffness map of membrane protein moieties estimated from thermal motion (Preiner et al 2015)
Diffusion and interaction of outer membrane protein F (OmpF) (Casuso et al 2012)
Bacteriorhodopsin responding to light (Shibata et al 2010; Yamashita et al 2013)
ATP-induced height change of Ca^{2+} pump (Yokokawa and Takeyasu 2011)
Molecular chaperones
Dynamic GroEL-GroES interaction (Yamamoto et al 2016)
Conformational change of AAA+ protein p97 coupled with the ATPase reaction (Noi et al 2013)
Enzymes
Unidirectional motion of cellulases on cellulose fibers (Igarashi et al 2011)
Two-way motion of chitinases on crystalline chitin (Igarasshi et al 2014)
Polarized movement of collagenase along collagen fibrils (Watanabe-Nakayama et al 2016)
Amyloid fibrils
Fibril formation by lithosthatine peptide (Milhiet et al 2010)
Fibril formation by amyloid β1-42 (Watanabe-Nakayama et al 2016)
Intrinsically disordered proteins
Structure of FACT protein and effect of phosphorylation (Miyagi et al 2008; Hashimoto et al 2013)
Two-ball structure of the flagellar hook-length control protein FliK (Kodera et al 2015)
Autophagy protein Atg13 undergoing order/disorder transitions (Yamamoto et al 2016)
Analysis of IDP structure at the residue level (*Kodera et al)
Cytoskeletons
Cofilin-induced unidirectional conformational changes in actin filaments (Ngo et al 2015)
Effect of inner microtubule proteins on the stability of doublet microtubules (*Owa et al)
Antibodies
Walking of antibodies on antigens arranged in lattice patterns (Preiner et al 2014)
DNA and DNA-binding proteins
Condensin smc2-smc4 dimers showing variety of conformations (Eeftens et al 2016)
Motion of DNA nano-robots (Rajendran et al 2015; Wickham et al 2011)
Oligomerization and dynamics of APOBEC3G interacting with DNA (Shlyakhtenko et al 2013)
Cells and Organelles
Moving net-like structure formed by prion covering living bacteria (Yamashita et al 2012; Oestreicher et al 2015)
Dynamic morphological changes in living cells (Shibata et al 2015)
Dynamics of nucleoporins inside nuclear porin complexes of Xenopus laevis oocytes (Sakiyama et al 2016)
Responses of bacteria to antimicrobial peptide (Fantner et al 2010)

*Personal communications

Figure-1

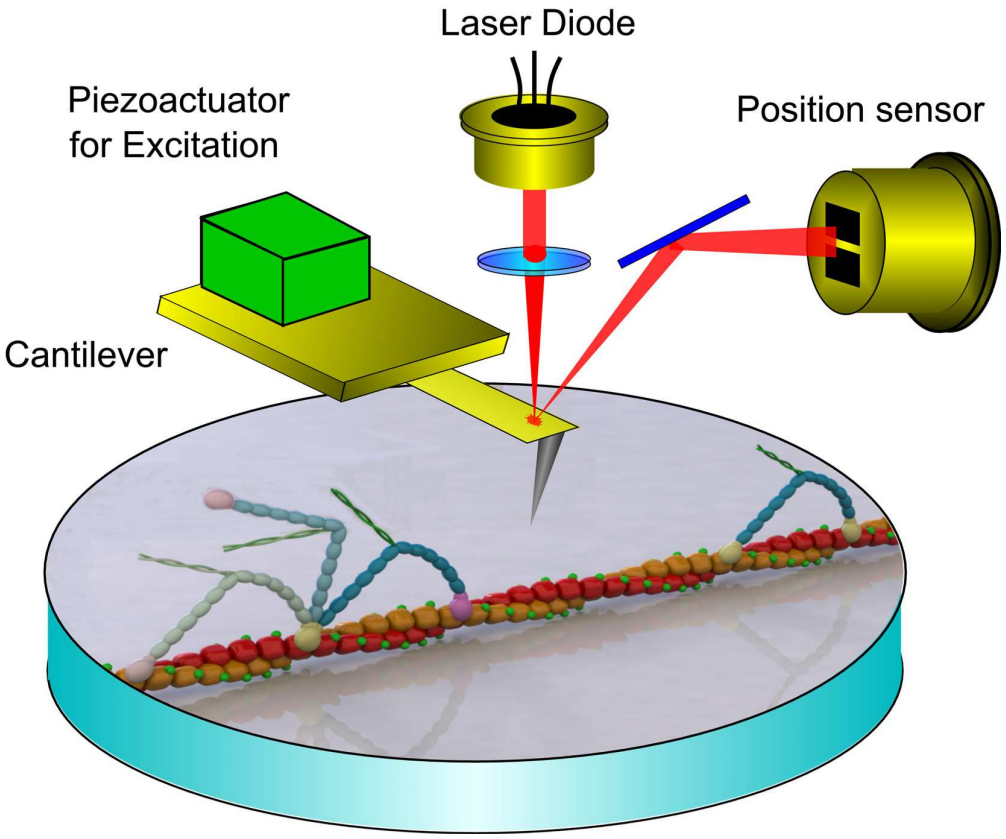
Laser Diode
Piezoactuator
for Excitation
Position sensor
Cantilever

Figure-2

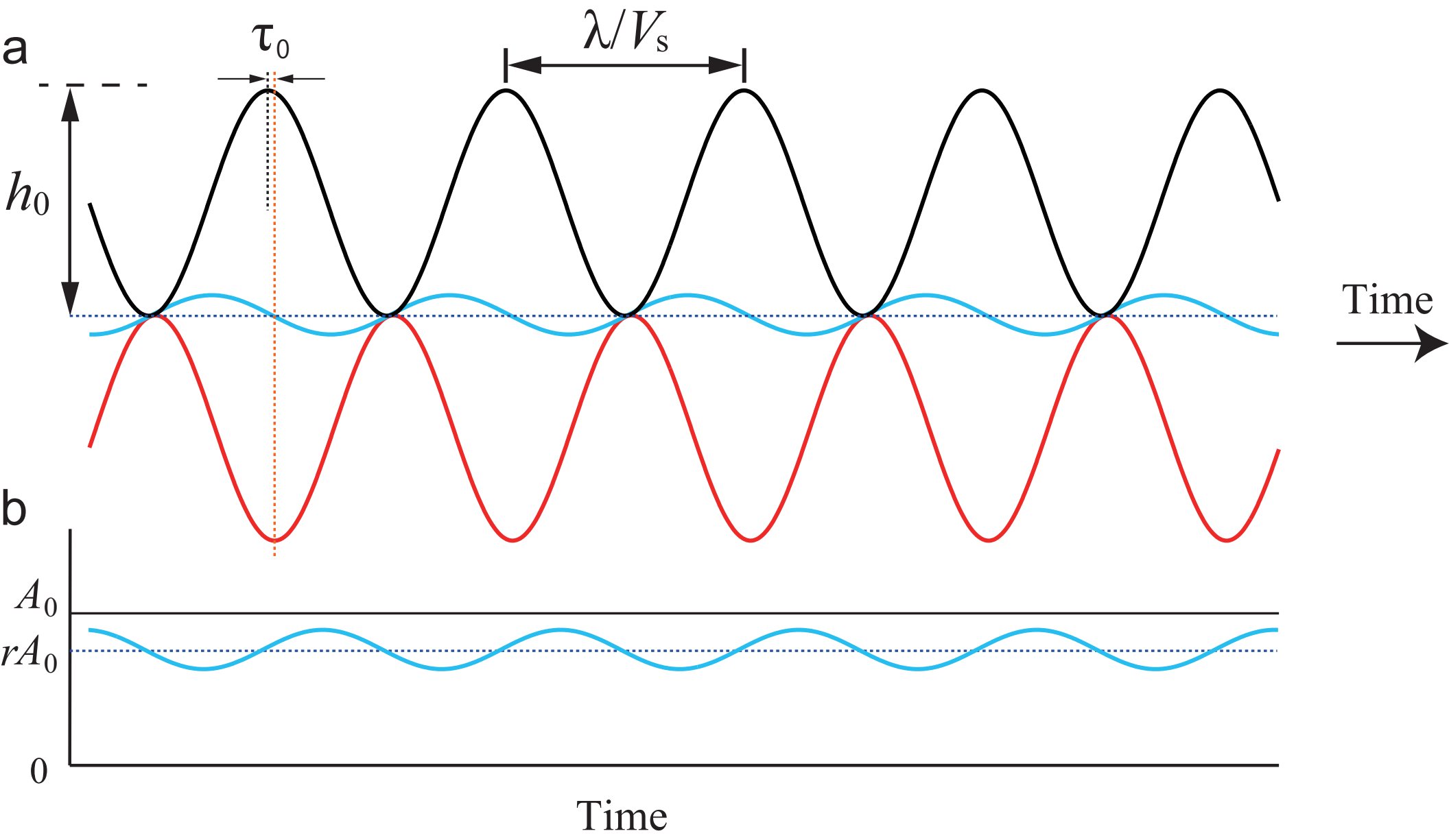

Figure-3

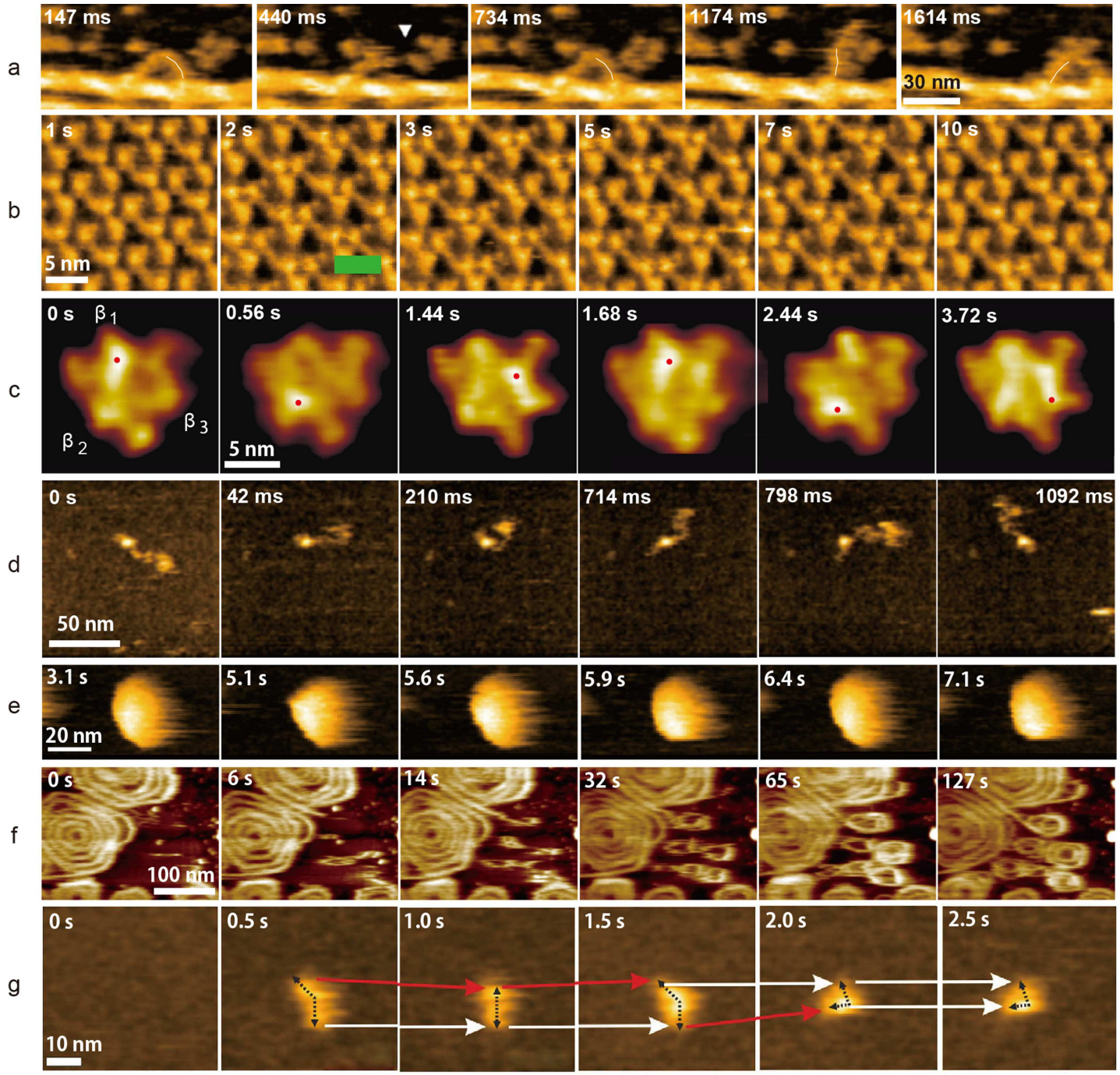
a
147 ms
440 ms
734 ms
1174 ms
1614 ms
30 nm
b
1 s
2 s
3 s
5 s
7 s
10 s
5 nm
c
0 s
β1
β2
β3
0.56 s
1.44 s
1.68 s
2.44 s
3.72 s
5 nm
d
0 s
42 ms
210 ms
714 ms
798 ms
1092 ms
50 nm
e
3.1 s
5.1 s
5.6 s
5.9 s
6.4 s
7.1 s
20 nm
f
0 s
6 s
14 s
32 s
65 s
127 s
100 nm
g
0 s
0.5 s
1.0 s
1.5 s
2.0 s
2.5 s
10 nm